1 of 6



Received: 21 June 2023 Revised: 10 July 2023 Accepted: 11 July 2023

# Optimal pore shape in a low-Pt PEM fuel cell cathode catalyst layer

# Andrei Kulikovsky<sup>1,2</sup>

<sup>1</sup>Theory and Computation of Energy Materials (IEK–13), Institute of Energy and Climate Research,

Forschungszentrum Jülich GmbH, Jülich, Germany

<sup>2</sup>Research Computing Center, Lomonosov Moscow State University, Moscow, Russia

# Correspondence

Email: A.Kulikovsky@fz-juelich.de

# **Abstract**

A model for performance of an axially symmetric pore with the curved generatrix is developed. Oxygen transport along the pore axis and in the radial direction through a thin ionomer film separating the pore volume from the Pt/C surface is taken into account. A performance functional is formulated, and the Euler–Lagrange equation is solved numerically for an optimal pore shape. This shape is close to a cubic paraboloid converging toward the membrane. Polarization curves show superior performance of the optimal pore over the cylindrical pore of the same active (side) surface area. The results suggest the shape of optimal ionomer loading for low-Pt electrodes.

#### KEYWORDS

low-Pt loading, modeling, oxygen transport, PEM fuel cell

# 1 | INTRODUCTION

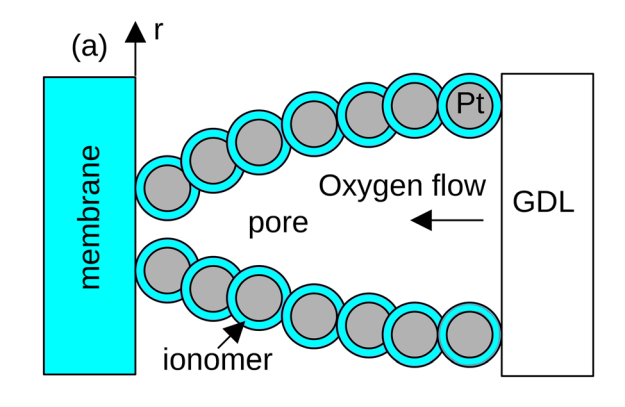
The success of polymer electrolyte membrane (PEM) fuel cells on the market of vehicle power sources to a large extent depends on the cells cost. To this end, reduction of Pt loading in the cathode catalyst layer is the problem of utmost importance.

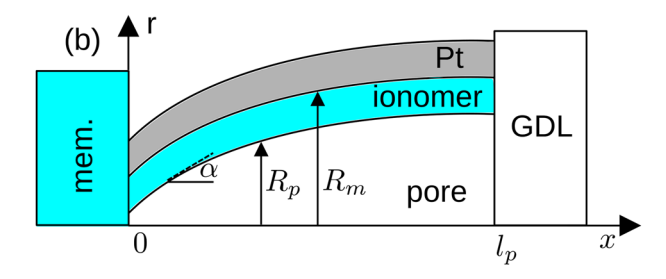
Low-Pt electrodes are the usually manufactured using the standard technique of Pt/C loading, just reducing the cathode catalyst layer (CCL) thickness. This means that the volumetric structure and morphology of low-Pt CCL do not differ much from those of the standard (thick) electrodes. Optimization of oxygen transport through a system of randomly oriented void pores formed by Pt/C agglomerates covered by a thin ionomer film is of paramount importance for low-Pt cell performance. [1–6] In the context of the present work, of particular interest are studies of CCLs with nonuniform (gradient) ionomer loading along the CCL depth.

Chen et al.<sup>[7]</sup> and Shahgaldi et al.<sup>[8]</sup> developed two-layer CCLs with a higher ionomer and Pt loadings close to the membrane. They demonstrated significant improvement of cell performance due to better oxygen transport through the two-layer systems. Xi et al. [9] studied three-layer systems and reported better performance of the electrode with Nafion content monotonically increasing toward the membrane e. Liao et al.[10] generated three-dimensional porous structures modeling real low-Pt CCL and used the lattice Boltzmann method to simulate oxygen transport through the structures. The effects of varying Pt, carbon, and ionomer content along the CCL thickness have been studied. Liao et al.[10] also performed numerical experiment with the oxygen transport through the perforated CCL. It was shown that cylindrical perforation of the radius 28 nm through the CCL thickness increases oxygen content close to the membrane by a factor of 2. Note that in their model, the variation of oxygen reduction reaction (ORR) overpotential through the CCL depth was ignored.

This is an open access article under the terms of the Creative Commons Attribution License, which permits use, distribution and reproduction in any medium, provided the original work is properly cited.

© 2023 The Authors. Electrochemical Science Advances published by Wiley-VCH GmbH.





(a) Schematic of a curved pore formed by Pt/C FIGURE 1 agglomerates covered by a thin ionomer film. (b) A model for the curved pore performance and the system of coordinates. Half of the axially symmetric pore is shown. GDL stands for the gas diffusion layer.

Below, a model for performance of an axially symmetric curved pore in the CCL is developed. The pore performance equations lead to the variational problem for an optimal pore shape. Numerical solution of this problem gives the "bullet"-like pore shape, which is well described by cubic parabola along the pore length. A polarization curve shows superior performance of the optimal pore compared to the cylindrical pore with the same side surface area.

#### 2 MODEL

The CCL is modeled by a single curved pore separated from the coaxial Pt/C surface by a thin ionomer film (Figure 1). The model employs the following basic assumptions:

- The catalyst layer is isothermal, i.e., there is no significant temperature gradient through the CCL thickness.
- · The pore is not flooded, meaning that the pore oxygen diffusivity does not change with the distance along the
- The thickness of ionomer film covering Pt/C agglomerates is constant along the pore.

· The ionomer film proton conductivity does not vary along the pore.

The conservation equations below are formulated using the following dimensionless variables:

$$\tilde{x} = \frac{x}{l_p}, \quad \tilde{r} = \frac{r}{l_p}, \quad \tilde{c} = \frac{c}{c_h^{in}}, \quad \tilde{j} = \frac{jl_p}{\sigma_N b}, \quad \tilde{\eta} = \frac{\eta}{b},$$

$$\tilde{D}_{ox} = \frac{4FD_{ox}c_h^{in}}{\sigma_N b}, \quad \tilde{D}_N = \frac{4FD_Nc_h^{in}}{\sigma_N b}, \quad (1)$$

where  $l_p$  is the pore length (CCL thickness),  $c_h^{in}$  is the reference (inlet) oxygen concentration,  $\sigma_N$  is the ionomer film proton conductivity, b is the ORR Tafel slope, j is the local proton current density,  $\eta$  is the cathode overpotential, positive by convention,  $D_{ox}$  is the oxygen diffusion coefficient in the pore, and  $D_N$  is the oxygen diffusivity of the ionomer film.

A model for electrochemical performance of a conical pore[11] leads to equations for the local oxygen concentration  $\tilde{c}$  in the pore and the local ORR overpotential  $\tilde{\eta}$ :

$$\varepsilon^2 \tilde{D}_{ox} \left( \frac{\partial^2 \tilde{c}}{\partial \tilde{x}^2} + \frac{2 \tan(\alpha)}{\tilde{R}_p} \frac{\partial \tilde{c}}{\partial \tilde{x}} \right) = \frac{K_H \tilde{c} \, e^{\tilde{\eta}}}{1 + \xi e^{\tilde{\eta}}}, \tag{2}$$

$$\varepsilon^2 \frac{\partial^2 \tilde{\eta}}{\partial \tilde{x}^2} = \frac{K_H \tilde{c} \, e^{\tilde{\eta}}}{1 + \xi e^{\tilde{\eta}}}.$$
 (3)

Here  $R_p(x)$  is the pore radius,  $K_H$  is the dimensionless Henry's constant for oxygen solubility in the ionomer,

$$\varepsilon = \sqrt{\frac{\sigma_N b}{i_* l_p^2}}, \quad \xi = \frac{\tilde{R}_p^2 \ln \left(\tilde{R}_m / \tilde{R}_p\right) \cos \alpha}{2\varepsilon^2 \tilde{D}_N}, \tag{4}$$

where  $i_*$  is the volumetric ORR exchange current density,  $R_m(x)$  is the metal radius, and  $\alpha(x)$  is the local pore angle (Figure 1b). The boundary conditions for Equations (2) and (3) are as follows:

$$\frac{\partial \tilde{c}}{\partial \tilde{x}}\Big|_{\tilde{x}=0} = 0, \quad \tilde{c}(1) = \tilde{c}_1,$$

$$\frac{\partial \tilde{\eta}}{\partial \tilde{x}}\Big|_{\tilde{x}=0} = -\tilde{j}_0, \quad \frac{\partial \tilde{\eta}}{\partial \tilde{x}}\Big|_{\tilde{x}=1} = 0, \quad (5)$$

where  $\tilde{c}_1$  is the oxygen concentration at the pore/GDL interface and  $\tilde{j}_0$  is the cell current density.

Any axially symmetric pore of an arbitrary shape can be approximated using small conoid elements. It follows that



Equation (2) also describes the oxygen transport in a pore of an arbitrary curved shape, provided that the functions  $\alpha(x)$  and  $R_p(x)$  describing the pore generatrix are given. Further, simple geometry shows that for a curved pore

$$t \equiv \tan \alpha = \frac{\partial \tilde{R}_p}{\partial \tilde{x}}.$$
 (6)

The ionomer film thickness  $\tilde{l}_N$  is typically much less than the pore radius, and we can simplify  $\xi$ , Equation (4), as the following:

$$\xi = \frac{\tilde{R}_p^2 \ln \left( (\tilde{R}_p + \tilde{l}_N) / \tilde{R}_p \right) \cos \alpha}{2 \varepsilon^2 \tilde{D}_N} \simeq \frac{\tilde{R}_p \tilde{l}_N \cos \alpha}{2 \varepsilon^2 \tilde{D}_N}.$$

Further, since  $\alpha = \arctan(t)$ , for  $\xi$  we finally find

$$\xi(\tilde{R}_p, t) = \frac{a\tilde{R}_p}{\sqrt{1 + t^2}}, \quad a = \frac{\tilde{l}_N}{2\varepsilon^2 \tilde{D}_N}.$$
 (7)

The right side of Equations (2) and (3) is the expression for the local ORR rate including oxygen dissolution in the ionomer film and radial oxygen transport through the film to the Pt/C surface (Figure 1). Thus, the total proton current density  $\tilde{j}_0$  converted in the pore is given by

$$\tilde{j}_0 = \int_0^1 \frac{K_H \tilde{c} \, e^{\tilde{\eta}}}{1 + \xi e^{\tilde{\eta}}} \, d\tilde{x} = K_H \int_0^1 \frac{\tilde{c} \, d\tilde{x}}{e^{-\tilde{\eta}} + \xi}. \tag{8}$$

The right side of Equation (8) can be considered as a functional of  $\tilde{R}_{p}(\tilde{x})$ . Indeed, from Equations (2) and (3) it is clear that  $\tilde{c} = \tilde{c}(\tilde{R}_p, t)$  and  $\tilde{\eta} = \tilde{\eta}(\tilde{R}_p, t)$ . We, thus, can formulate the following optimization problem: find the optimal shape  $\tilde{R}_{D}(\tilde{x})$ , maximizing the functional (8):

$$\int_{0}^{1} L(\tilde{x}, \tilde{R}_{p}, t) d\tilde{x} \to \max$$
 (9)

where L is the expression under integral in Equation (8)

$$L = \frac{\tilde{c}(\tilde{R}_p, t)}{\exp(-\tilde{\eta}(\tilde{R}_p, t)) + \xi(\tilde{R}_p, t)}.$$
 (10)

Below, the subscript p will be omitted,  $\tilde{R} \equiv \tilde{R}_p$ .

The Euler-Lagrange equation for the problem Equation (9) is

$$\frac{\partial L}{\partial \tilde{R}} - \frac{\partial}{\partial \tilde{x}} \left( \frac{\partial L}{\partial t} \right) = 0. \tag{11}$$

Differentiating Equation (10) over  $\tilde{R}$  and making substitutions  $\partial \tilde{y}/\partial \tilde{R} = (\partial \tilde{y}/\partial \tilde{x})/(\partial \tilde{R}/\partial \tilde{x}), \ \tilde{y} = \{\tilde{c}, \tilde{\eta}\}\$ , we get the first term in Equation (11)

$$\begin{split} \frac{\partial L}{\partial \tilde{R}} &= \frac{\tilde{c} \, \mathrm{e}^{-\tilde{\eta}} \partial \tilde{\eta} / \partial \tilde{x}}{\left( \mathrm{e}^{-\tilde{\eta}} + a \tilde{R} / \sqrt{1 + t^2} \right)^2 \partial \tilde{R} / \partial \tilde{x}} \\ &+ \frac{\partial \tilde{c} / \partial \tilde{x}}{\left( \mathrm{e}^{-\tilde{\eta}} + a \tilde{R} / \sqrt{1 + t^2} \right) \partial \tilde{R} / \partial \tilde{x}} \\ &- \frac{a \tilde{c}}{\left( \mathrm{e}^{-\tilde{\eta}} + a \tilde{R} / \sqrt{1 + t^2} \right)^2 \sqrt{1 + t^2}}. \end{split} \tag{12}$$

For the derivative  $\partial L/\partial t$  in Equation (11), we find

$$\frac{\partial L}{\partial t} = \frac{\tilde{c} e^{-\eta} \partial \tilde{\eta} / \partial \tilde{x}}{\left(e^{-\tilde{\eta}} + a\tilde{R} / \sqrt{1 + t^2}\right)^2 \partial t / \partial \tilde{x}} + \frac{\partial \tilde{c} / \partial \tilde{x}}{\left(e^{-\tilde{\eta}} + a\tilde{R} / \sqrt{1 + t^2}\right) \partial t / \partial \tilde{x}} + \frac{a\tilde{c}\tilde{R}t}{\left(e^{-\tilde{\eta}} + a\tilde{R} / \sqrt{1 + t^2}\right)^2 (1 + t^2)^{3/2}}. \tag{13}$$

Substitution of Equations (12) and (13) into the Euler-Lagrange equation (11) and noting that  $t(x) = \partial \tilde{R} / \partial \tilde{x}$  leads to the third-order ordinary differential equation (ODE) for  $\tilde{R}(\tilde{x})$  of the form

$$\frac{\partial^3 \tilde{R}}{\partial \tilde{x}^3} = \left(\frac{\partial^2 \tilde{R}/\partial \tilde{x}^2}{\partial \tilde{R}/\partial \tilde{x}}\right) \frac{N_3}{D_3},\tag{14}$$

where the factors  $N_3$  and  $D_3$  are given in the Appendix. The optimal pore shape is determined by the system of Equations (2), (3), and (14).

# RESULTS AND DISCUSSION

Equation (14) requires three boundary conditions; here, we set the inlet and outlet pore radii and zero derivative of the pore radius over  $\tilde{x}$  at the pore inlet:

$$\tilde{R}(0) = \tilde{R}_0, \quad \tilde{R}(1) = \tilde{R}_1, \quad \frac{\partial \tilde{R}}{\partial \tilde{x}} \Big|_{\tilde{x}=1} = 0,$$
 (15)

where the subscripts 0 and 1 refer to the membrane/pore and pore/GDL interfaces, respectively. It has been shown[11] that the conical pore converging toward the membrane outperforms the cylindrical pore with the same side surface area (active surface area). The results below

 TABLE 1
 Pore/cell geometrical and operating parameters.

THE E TOTO, con geometrical and operating parameters.	
Pore length $l_p$ , $\mu$ m	3
Inlet pore radius (CCL/GDL), $R_1$ , nm	32.2
Outlet pore radius (membrane/CCL) $R_0$ , nm	3.22
Nafion film thickness $l_N$ , nm	10
ORR exchange current density	
$i_*$ , A cm <sup>-3</sup>	$10^{-3}$
Henry's constant for oxygen solubility	
in water at 80°C, mol mol <sup>-1</sup>	$6.76\cdot10^{-3}$
ORR Tafel slope $b$ , V	0.03
Ionomer proton conductivity,	
$\sigma_N$ , mS cm $^{-1}$	2
Double layer capacitance $C_{dl}$ , F cm <sup>-3</sup>	20
Relative humidity	50%
Cathode absolute pressure, kPa	150
Cell temperature, K	273 + 80

were calculated with  $\tilde{R}_1 = 32.2$  nm, which is the mean pore radius of a standard Gore Pt/C electrode<sup>[12]</sup> and  $\tilde{R}_0 = \tilde{R}_1/10$ , that is, the optimal pore shape was sought among the shapes converging toward the membrane.

The von Neumann boundary condition  $\partial \tilde{R}/\partial \tilde{x}|_{\tilde{x}=1}=0$  poses a problem in numerical solution of Equation (14). Indeed, the derivative  $\partial \tilde{R}/\partial \tilde{x}$  appears as a factor in the denominator of the right side, meaning the singularity at  $\tilde{x}=1$ . To resolve the problem, a small term  $\epsilon=10^{-8}$  was added as shown in Equation (16)

$$\frac{\partial^3 \tilde{R}}{\partial \tilde{x}^3} = \left(\frac{\partial^2 \tilde{R}/\partial \tilde{x}^2}{\partial \tilde{R}/\partial \tilde{x} + \epsilon}\right) \frac{N_3}{D_3}.$$
 (16)

The derivative  $\partial \tilde{R}/\partial \tilde{x}$  rapidly grows with the distance from  $\tilde{x} = 1$ , and small  $\varepsilon$  corrects the solution in a small range  $1 - \sqrt[3]{\varepsilon} \lesssim \tilde{x} \leq 1$  only.

Equations (2), (3), and (16) were solved numerically using the boundary-value problem solver solve\_bvp from the Python SciPy library. Parameters used for calculations are listed in Table 1. The results for the cell current density of 1.5 A cm<sup>-2</sup> are shown in Figure 2. The optimal "bullet"-like pore shape is nearly independent of the cell current density, and it is close to a cubic parabola (points in Figure 2b) with the parameters indicated in the caption to Figure 2. The shapes of the oxygen concentration and overpotential along the optimal pore are compared with these shapes for the cylindrical poreof the same side surface area (electrochemically active surface area). As can be seen, oxygen transport in the optimal pore is significantly improved leading to lower total potential loss ( $\eta(0)$  at the membrane surface). The gain in voltage loss is about 60 mV (Figure 2a).

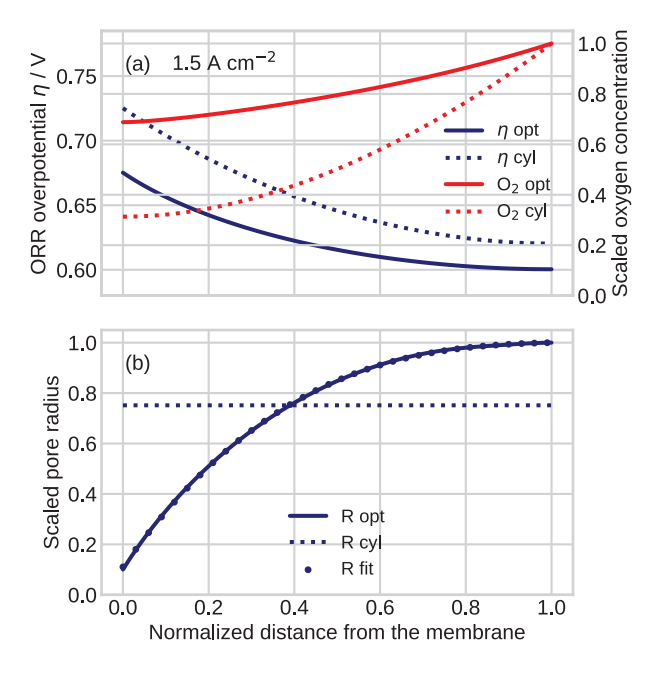
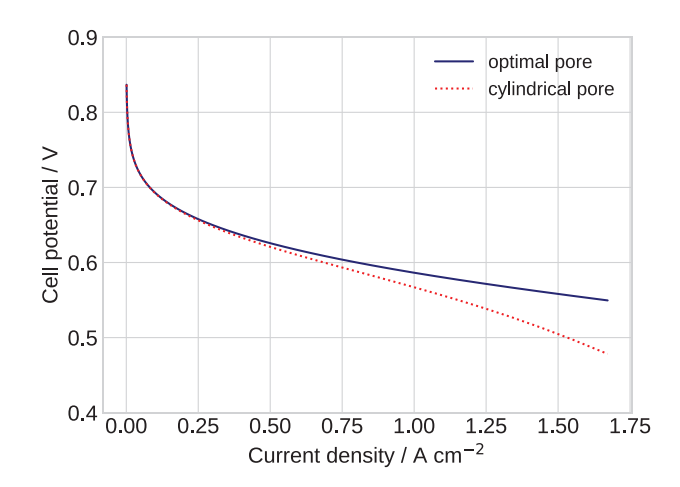


FIGURE 2 (a) ORR overpotential (solid red line) and oxygen concentration (solid blue line) along the optimal pore for the cell current density of 1.5 A cm<sup>-2</sup>. Dotted lines: the same parameters along the cylindrical pore with the equivalent side surface area. (b) Solid line: the dependence of scaled optimal pore radius  $R_{opt}/R_1$  on the distance from the membrane, dotted line: the radius of cylindrical pore with equivalent side surface area. Points show the cubic parabola  $a\tilde{x}^3 + b\tilde{x}^2 + c\tilde{x} + d$  fitted to the scaled optimal pore radius, where a = 0.6457, b = -2.145, c = 2.389, and d = 0.1104. Note that in the dimension coordinates, the x-axis is about 30 times longer than the y-axis.



**FIGURE 3** Polarization curves of the optimal curved and equivalent cylindrical pores.

Figure 3 compares the polarization curves of the "bullet" pore and the equivalent cylindrical pore. For illustration purposes, the curves were calculated as  $V_{cell} = 1.23 - \eta_0$ , where  $\eta_0 \equiv \eta|_{x=0}$  is the total potential loss in the pore.

As can be seen, the optimal pore does not exhibit oxygen transport loss; in contrast, the cylindrical pore curve declines down at the current densities above 0.5 A cm<sup>-2</sup> due to poor oxygen transport (Figure 3).

Calculations show that simultaneous  $\pm 50\%$  variation of the inlet and outlet pore radii leads to a very close optimal pore shape. The shape in Figure 2b is also almost insensitive to the variation of the ORR Tafel slope.

Generally, an optimal pore not necessarily needs to be axially symmetric; a tortuous pore with the cross-sectional area lowering toward the membrane would give better performance. Pore tortuosity can be described by lowering of effective oxygen diffusivity  $D_{ox}$  and increasing pore length. Since pore-size distribution depends on ionomer loading, the positive effect of the "bullet" pore could be achieved by increasing ionomer loading toward the membrane. The pore shape in Figure 2b suggests the optimal ionomer volume fraction along the CCL thickness.

the oxygen concentration and overpotential along the pore length. Optimal pore shape is obtained from the numerical solution of this problem; the shape is well described by the cubic paraboloid converging toward the membrane. Polarization curves show superior performance of the optimal pore as compared to the cylindrical pore of equivalent side surface area. The results suggest the optimal shape of ionomer loading for the low-Pt CCL.

# APPENDIX A: FACTORS IN EQUATIONS (14) and (16)

Below, the following notations are used:

$$\tilde{R}_{\tilde{x}} \equiv \frac{\partial \tilde{R}}{\partial \tilde{x}}, \quad \tilde{R}_{\tilde{x}\tilde{x}} \equiv \frac{\partial^2 \tilde{R}}{\partial \tilde{x}^2}$$
 (A1)

and similar for the  $\tilde{x}$ -derivatives of  $\tilde{c}$  and  $\tilde{\eta}$ .

$$\begin{split} N_{3} &= \left(\tilde{R}_{\tilde{\chi}}^{2} + 1\right)^{3} \left(\left(\tilde{c}\tilde{\eta}_{\tilde{\chi}}^{2} + \tilde{c}\tilde{\eta}_{\tilde{\chi}\tilde{\chi}} + 2\tilde{c}_{\tilde{\chi}}\tilde{\eta}_{\tilde{\chi}} + \tilde{c}_{\tilde{\chi}\tilde{\chi}}\right)\tilde{R}_{\tilde{\chi}} - \tilde{R}_{\tilde{\chi}\tilde{\chi}}\tilde{c}\tilde{\eta}_{\tilde{\chi}} - \tilde{R}_{\tilde{\chi}\tilde{\chi}}\tilde{c}_{\tilde{\chi}}\right) \mathrm{e}^{-2\eta} \\ &+ a\sqrt{\tilde{R}_{\tilde{\chi}}^{2} + 1} \left(\left(\left(\tilde{R}_{\tilde{\chi}}^{2} + 1\right)\tilde{R}\tilde{c}\tilde{R}_{\tilde{\chi}} - 3\tilde{R}\tilde{c}\tilde{R}_{\tilde{\chi}}^{3}\right)\tilde{R}_{\tilde{\chi}\tilde{\chi}}^{2} + \left(\tilde{R}_{\tilde{\chi}}^{2} + 1\right)\left(3\tilde{R}\tilde{R}_{\tilde{\chi}}^{2}\tilde{c}\tilde{\eta}_{\tilde{\chi}} + 2\tilde{R}_{\tilde{\chi}}^{3}\tilde{c} - \tilde{R}\tilde{c}\tilde{\eta}_{\tilde{\chi}} - 2\tilde{R}\tilde{c}_{\tilde{\chi}} + \tilde{R}_{\tilde{\chi}}\tilde{c}\right)\tilde{R}_{\tilde{\chi}\tilde{\chi}} \right. \\ &- \left(\tilde{R}_{\tilde{\chi}}^{2} + 1\right)^{2}\tilde{R}_{\tilde{\chi}}\left(\left(2\tilde{c}\tilde{\eta}_{\tilde{\chi}} + \tilde{c}_{\tilde{\chi}}\right)\tilde{R}_{\tilde{\chi}} + \left(\tilde{c}\tilde{\eta}_{\tilde{\chi}}^{2} - \tilde{c}\tilde{\eta}_{\tilde{\chi}\tilde{\chi}} - 2\tilde{c}_{\tilde{\chi}}\tilde{\eta}_{\tilde{\chi}} - 2\tilde{c}_{\tilde{\chi}\tilde{\chi}}\right)\tilde{R}\right)\right)\mathrm{e}^{-\tilde{\eta}} \\ &+ a^{2}\tilde{R}\left(\tilde{R}\tilde{c}\tilde{R}_{\tilde{\chi}}\tilde{R}_{\tilde{\chi}\tilde{\chi}}^{2} + \left(\tilde{R}\tilde{R}_{\tilde{\chi}}^{4}\tilde{c}_{\tilde{\chi}} + \tilde{R}_{\tilde{\chi}}^{3}\tilde{c} - \tilde{R}\tilde{c}_{\tilde{\chi}} + \tilde{R}_{\tilde{\chi}}\tilde{c}\right)\tilde{R}_{\tilde{\chi}\tilde{\chi}} + \tilde{R}_{\tilde{\chi}}\left(\tilde{R}_{\tilde{\chi}}^{2} + 1\right)^{2}\left(\tilde{R}\tilde{c}_{\tilde{\chi}\tilde{\chi}} - \tilde{R}_{\tilde{\chi}}\tilde{c}_{\tilde{\chi}}\right)\right) \quad (A2) \end{split}$$

Note that the model above is based on the assumption of constant along x ionomer proton conductivity  $\sigma_N$ , while variation of ionomer loading through the CCL depth would lead to variable  $\sigma_N(x)$ . However, numerous works suggest that the main reason for reduced performance of low-Pt electrodes is oxygen transport. Figure 3 shows that the "bullet" pore solves this problem, and hence the best option would be engineering a system of parallel, axially symmetric curved nanopores using pore formers or a special perforator.

# 4 | CONCLUSIONS

A model for performance of an axially symmetric curved pore for the low-Pt cathode catalyst layer is developed. The oxygen transport along the pore and through a thin ionomer film separating the pore from the Pt/C surface is taken into account. The total proton current converted in the pore is a functional of the pore shape. The Euler–Lagrange equation for the optimal shape leads to the third-order ODE for pore radius, coupled to the ODEs for

$$\begin{split} D_3 &= \left(a \mathrm{e}^{-\tilde{\eta}} \tilde{R} (\tilde{\eta}_{\tilde{x}} \tilde{c} + 2 \tilde{c}_{\tilde{x}}) \sqrt{\tilde{R}_{\tilde{x}}^2 + 1} \right. \\ &+ \left(\tilde{R}_{\tilde{x}}^2 + 1\right) (\tilde{\eta}_{\tilde{x}} \tilde{c} + \tilde{c}_{\tilde{x}}) \mathrm{e}^{-2\tilde{\eta}} + a^2 \tilde{R}^2 \tilde{c}_{\tilde{x}} \right) \left(\tilde{R}_{\tilde{x}}^2 + 1\right)^2. \text{ (A3)} \end{split}$$

# **NOMENCLATURE**

- Marks dimensionless variables
- a Dimensionless parameters, Equation (7)
- b ORR Tafel slope, V
- c Oxygen molar concentration in the pore, mol cm $^{-3}$
- $c_N$  Dissolved oxygen molar concentration in the ionomer, mol cm<sup>-3</sup>
- $c_h^{in}$  Reference (inlet) oxygen concentration, mol cm $^{-3}$
- $D_{ox}$  Oxygen diffusion coefficient in the pore, cm<sup>2</sup> s<sup>-1</sup>
- $D_N$  Oxygen diffusion coefficient in the ionomer, cm<sup>2</sup> s<sup>-1</sup>
- F Faraday constant, C  $mol^{-1}$
- $i_*$  ORR volumetric exchange current density, A cm<sup>-3</sup>

urch Center, Wiley Online Library on [23/08/2024]. See the Terms

- $i_0$  Cell current density, A cm<sup>-2</sup>
- Local proton current density in the film, A cm<sup>-2</sup>
- $K_H$  Dimensionless Henry's constant for oxygen dissolution in the ionomer, mol/mol
  - Dimensionless functional, Equation (10)
- Pore (CCL) length, cm
- $R_{n}$ Pore radius, cm
- $R_m$  Pt/C radius, cm
  - r Radial coordinate, cm
  - $t \quad t \equiv \tan \alpha = \partial R_p / \partial x$
  - x Coordinate along the pore, cm

# **Subscripts:**

- 0 Membrane/pore interface
- Pore/GDL interface
- Ionomer film

# Greek:

- Pore generatrix angle, rad
- ORR overpotential, positive by convention, V
- Dimensionless parameter, Equation (4)
- Ionomer film proton conductivity, S cm<sup>-1</sup>  $\sigma_N$
- ξ Dimensionless parameter, Equation (4)

# ACKNOWLEDGMENTS

Open access funding enabled and organized by Projekt DEAL.

### CONFLICT OF INTEREST STATEMENT

The author declares no conflict of interest.

# DATA AVAILABILITY STATEMENT

Data sharing is not applicable—no new data are generated, or the article describes entirely theoretical research.

#### ORCID

Andrei Kulikovsky https://orcid.org/0000-0003-1319-

#### REFERENCES

- 1. D. R. Baker, D. A. Caulk, K. C. Neverlin, M. W. Murphy, J. Electrochem. Soc. 2009, 156, B991.
- 2. S. Sambandam, J. Parrondo, V. Ramani, Phys. Chem. Chem. Phys. 2013, 15, 14994.
- 3. T. Suzuki, K. Kudo, Y. Morimoto, J. Power Sources 2013, 222, 379.
- 4. J. Liang, Y. Li, R. Wang, J. Jiang, Chem. Eng. J. 2020, 400, 125796.
- 5. R. Darling, S. F. Burlatsky, J. Electrochem. Soc. 2020, 167, 104506.
- 6. S. Mizuno, S. Uemura, Y. Tabe, ECS Trans. 2021, 104, 175.
- 7. G.-Y. Chen, C. Wang, Y.-J. Lei, J. Zhang, Z. Mao, Z.-Q. Mao, J.-W. Guo, J. Li, M. Ouyang, Int. J. Hydrogen Energy 2017, 42, 29960.
- 8. S. Shahgaldi, A. Ozden, X. Li, F. Hamdullahpur, Energy Conv. Management 2018, 171, 1476.
- 9. Z. Xie, T. Navessin, K. Shi, R. Chow, Q. Wang, D. Song, B. Andreaus, M. Eikerling, Z. Liu, S. Holdcroft, J. Electrochem. Soc. 2005, 152, A1171.
- 10. J. Liao, G. Yang, Q. Shen, S. Li, Z. Jiang, H. Wang, G. Zhang, Z. Li, N. Huang, Mat. Today Comm. 2023, 35, 106304.
- 11. A. Kulikovsky, Electrochem. Sci. Adv. 2023. https://doi.org/10. 1002/elsa.202300006
- 12. H. Yu, L. Bonville, R. Maric, J. Electrochem. Soc. 2018, 165, F272.

How to cite this article: A. Kulikovsky, Electrochem. Sci. Adv. 2024, 4, e202300021. https://doi.org/10.1002/elsa.202300021